International Journal of Thermophysics, Vol. 27, No. 2, March 2006 (© 2006)
DOI: 10.1007/s10765-005-0006-1

Analysis for Microscopic Hyperbolic Two-Step Heat Transfer Problems

Kuo-Chi Liu[1]

Received June 20, 2005

This work analyzes the heat transfer problems in thin metal films using the microscopic hyperbolic two-step model. It is necessary in dealing with such problems to solve a set of the coupled energy equations or an equation containing higher-order mixed derivatives in both time and space. This present numerical scheme eliminates the coupling between energy equations with the Laplace transform technique and leads to a second-order governing differential equation in the transform domain. Afterward, the transformed second-order governing differential equation is discretized by the control volume scheme. To demonstrate the efficiency and accuracy of the present numerical scheme, a comparison between the present numerical results and the analytical solution is made. Theoretical insight into the hyperbolic two-step heat conduction is provided. Results show that the thermal propagation velocity is finite and is independent of the coupling factor and the volumetric heat capacity ratio between electrons and the lattice.

KEY WORDS: ballistic behavior; high-rate heating; hybrid numerical scheme; hyperbolic two-step model.

1. INTRODUCTION

The use of high-rate heating on thin films is rapidly developing in micromachining, laser processing of diamond films, laser hardening, and other applications, due to the advancement of short-pulse energy deposition technologies. The energy pulse can be deposited over a duration of femtoseconds [1–3]. When such an energy pulse heats a thin metal film, the response time of the film is comparable to the phonon–electron thermalization time. Under such conditions, classical heat conduction models,

[1] Department of Mechanical Engineering, Far East College, 49 Chung Hua Rd., Hsin-Shih Tainan Prefecture, Taiwan 744, Republic of China. E-mail: kcliu@cc.fec.edu.tw

assuming thermal equilibrium between the solid lattice and electron gas, lose validity. Thus, Kaganov et al. [4] described the phenomena of energy interchange between electrons and phonons from a microscopic point of view. Anisimov et al. [5] derived the resulting phenomenological two-step model that is called the parabolic two-step heat conduction model, which has attracted attention in the analysis of micro-scale heat transfer [6–11]. However, as the response time is comparable or less than the relaxation time that is the characteristic time for the activation of ballistic behavior in the electron gas, the parabolic two-step model may lose accuracy [12, 13]. The relaxation time increases dramatically as the temperature decreases (from 0.04 ps at room temperature to about 10 ps at 10 K) [9]. Therefore, Qiu and Tien [12] proposed the hyperbolic two-step heat conduction model based on the macroscopic averages of the electric and heat currents carried by electrons in the momentum space. This model has been a satisfactory extension of the parabolic two-step model.

The solution of the coupled energy equations in the microscopic hyperbolic two-step model is difficult, even after eliminating the coupling, since the resulting equation contains higher-order mixed derivatives in both time and space and leads to complications in the solution procedures [14]. Thus, only a few studies [14–17] for theoretical predictions of the hyperbolic two-step heat conduction are available in the literature for some specific cases. For convenience of analysis, Al-Nimr and Arpaci [14] considered that the thermal behavior in thin metal films occurs in two separate stages. The first stage is very short and is described with the hyperbolic two-step model excluding the diffusion term. The second stage is described with the hyperbolic one-step model. Al-Nimr et al. [15] used a perturbation technique to analyze the distribution of both electron and lattice temperatures in a semiconductor film induced with the application of a strong energy pulse. However, the results do not completely satisfy the boundary conditions. The effect of high frequency fluctuating boundary heating on the hyperbolic two-step model was investigated with the complex method in Ref. [16]. In addition, the effect of the initial conditions of the lattice on the overshooting phenomenon was explored in Ref. [17] assuming that the effect from the initial conditions of the electron gas was ignored.

This work employs a hybrid application of the Laplace transform technique and the control volume method to solve various hyperbolic two-step heat conduction problems. The time-dependent terms in the governing differential equations and boundary conditions can be removed with the Laplace transform method. Thus, the coupling between the energy equations of the hyperbolic two-step model is eliminated. A second-order governing differential equation in the transform domain is obtained. The control volume scheme in conjunction with the approximation functions,

which are derived from a corresponding differential equation of the governing equation in the transform domain, is applied to discretize the resulting second-order differential equation.

2. MATHEMATICAL FORMULATION

Energy conservation equations and the heat flux equation for the hyperbolic two-step heat conduction model with the constant thermal properties are written as [12]

$$C_{\mathrm{e}}\frac{\partial T_{\mathrm{e}}}{\partial t} = -\frac{\partial q}{\partial x} - G(T_{\mathrm{e}} - T_{\mathrm{l}}) + S, \tag{1a}$$

$$C_{\mathrm{l}}\frac{\partial T_{\mathrm{l}}}{\partial t} = G(T_{\mathrm{e}} - T_{\mathrm{l}}), \tag{1b}$$

$$\tau\frac{\partial q}{\partial t} + k\frac{\partial T_{\mathrm{e}}}{\partial x} + q = 0, \tag{1c}$$

where C is the volumetric heat capacity, G is the coupling factor, k is the thermal conductivity, q is the heat flux, S is the radiation heating source, T is the temperature, t is the time, x is the space coordinate, and τ is the relaxation time. The subscripts e and l represent electron and lattice, respectively. Qiu and Tien [12] derived these equations under the assumptions that there is no electrical current during laser heating, that the electron gas totally absorbed the incident radiation, and that the thermal conductivity is completely contributed by the electron gas. The hyperbolic nature of energy transport by electrons is shown in Eq. (1c). The propagation speed of the thermal signal may be defined as $V = \sqrt{k/(C_{\mathrm{e}}\tau)}$, in accordance with that for the hyperbolic one-step model. The $\tau\frac{\partial q}{\partial t}$ term in Eq. (1c) can be neglected as the value of the relaxation time τ is sufficiently small, and then Eqs. (1a)–(1c) will become the equations of the parabolic two-step model.

For convenience of analysis, the dimensionless parameters are defined as

$$\theta = \frac{T - T_0}{T_{\mathrm{r}}}, \quad \eta = \frac{x}{\sqrt{k\tau/C_{\mathrm{e}}}}, \quad \xi = \frac{t}{\tau}, \quad Q = \frac{q}{T_{\mathrm{r}}\sqrt{kC_{\mathrm{e}}/\tau}},$$
$$E = \frac{S\tau}{C_{\mathrm{e}}T_{\mathrm{r}}}, \quad N = \frac{G\tau}{C_{\mathrm{e}}}, \quad \text{and} \quad R_{\mathrm{C}} = \frac{C_{\mathrm{l}}}{C_{\mathrm{e}}}, \tag{2}$$

where T_0 is the initial temperature and T_{r} is the reference temperature.

Substituting the dimensionless parameters in Eq. (2) into Eqs. (1a)–(1c) produces the dimensionless governing equations as

$$\frac{\partial \theta_e}{\partial \xi} = -\frac{\partial Q}{\partial \eta} - N(\theta_e - \theta_l) + E, \tag{3a}$$

$$R_C \frac{\partial \theta_l}{\partial \xi} = N(\theta_e - \theta_l), \tag{3b}$$

$$\frac{\partial Q}{\partial \xi} + Q = -\frac{\partial \theta_e}{\partial \eta}. \tag{3c}$$

The combination of Eqs. (3a)–(3c) leads to the following equation:

$$\frac{R_C}{N}\frac{\partial^3 \theta_l}{\partial \eta^2 \partial \xi} + \frac{\partial^2 \theta_l}{\partial \eta^2} = \frac{R_C}{N}\frac{\partial^3 \theta_l}{\partial \xi^3} + \left[1 + R_C + \frac{R_C}{N}\right]\frac{\partial^2 \theta_l}{\partial \xi^2} + [1 + R_C]\frac{\partial \theta_l}{\partial \xi} - \frac{\partial E}{\partial \xi} - E. \tag{4}$$

It can be easily observed that Eq. (4) contains higher-order mixed derivatives in both time and space. Some mathematical techniques must be applied to obtain an analytical solution of Eq. (4). Tzou [13, 18–20] has developed an analytical solution for the relevant problems using the Laplace transform.

The initial conditions of the problems illustrated in this work are given as

$$\theta_e(\eta, 0) = \theta_l(\eta, 0) = 0 \quad \text{and} \quad Q(\eta, 0) = 0. \tag{5}$$

The boundary conditions for the present problems will be discussed later.

3. NUMERICAL ANALYSIS

The Laplace transform technique is applied to remove the time-dependent terms from Eqs. (4a)–(4c). The Laplace transform is defined as

$$\tilde{\phi}(s) = \int_0^\infty \phi(\xi) e^{-s\xi} d\xi, \tag{6}$$

where s is the Laplace transform parameter. As the Laplace transformation of the heating source function E can be obtained, Eqs. (3a)–(3c) are written in the transform domain, respectively, as

$$\frac{d\widetilde{Q}}{d\eta} = -(s+N)\widetilde{\theta}_{\mathrm{e}} + N\widetilde{\theta}_{\mathrm{l}} + \widetilde{E}, \tag{7a}$$

$$\widetilde{\theta}_{\mathrm{l}} = \frac{N}{R_{\mathrm{C}}s+N}\widetilde{\theta}_{\mathrm{e}}, \tag{7b}$$

$$\frac{d\widetilde{\theta}_{\mathrm{e}}}{d\eta} = -(s+1)\widetilde{Q}. \tag{7c}$$

Rearrangement of Eqs. (7a)–(7c) leads to the equations,

$$\frac{d^2\widetilde{\theta}_{\mathrm{e}}}{d\eta^2} - \beta^2\widetilde{\theta}_{\mathrm{e}} = -(s+1)\widetilde{E}, \tag{8a}$$

and

$$\frac{d^2\widetilde{\theta}_{l}}{d\eta^2} - \beta^2\widetilde{\theta}_{l} = -\frac{N(s+1)}{R_C s+N}\widetilde{E}, \tag{8b}$$

where

$$\beta = \left[(s^2+s) + N(s+1) - \frac{N^2(s+1)}{R_C s+N}\right]^{1/2}. \tag{9}$$

In conjunction with the boundary conditions, the dimensionless electron temperature distribution can be analyzed with Eq. (8a). Similarly, using Eq. (8b) the dimensionless lattice temperature distribution can be directly analyzed. For convenience, in the subsequent analysis, Eqs. (8a) and (8b) are expressed in one form as

$$\frac{d^2\widetilde{\theta}}{d\eta^2} - \beta^2\widetilde{\theta} + \widetilde{H} = 0, \tag{10}$$

where

$$\widetilde{H} = (s+1)\widetilde{E}, \quad \text{for Eq. (8a)} \tag{11a}$$

and

$$\widetilde{H} = \frac{N(s+1)}{R_{\mathrm{C}}s+N}\widetilde{E}. \quad \text{for Eq. (8b)} \tag{11b}$$

Subsequently, Eq. (10) is discretized using the control volume method. Integration of Eq. (10) within a small control volume can be written as

$$\int_{\eta_i-\ell/2}^{\eta_i+\ell/2} \left\{ \frac{d^2\widetilde{\theta}}{d\eta^2} - \beta^2\widetilde{\theta} + \widetilde{H} \right\} d\eta = 0 \tag{12}$$

where ℓ is the distance between neighboring nodes. Before performing the integration of Eq. (12), the selection of an approximation function for $\widetilde{\theta}$ is important in order to have more accurate numerical results. Traditionally, the variable temperature distribution is linearly interpolated between the nodes [21]. To suppress the numerical oscillations encountered in non-Fickian mass diffusion problems, Chen and Liu [22–24] derived the approximation functions from the associated differential equation in the transform domain. Results in the previous studies [22–24] show that a good selection of the approximation functions is important to obtain accurate numerical results. A general solution of the corresponding homogeneous equation of Eq. (10) is

$$\widetilde{\theta} = A\cosh\beta\eta + B\sinh\beta\eta, \tag{13}$$

where the coefficients A and B are determined with the boundary conditions. The approximation function for $\widetilde{\theta}$ in this work, thus, is considered as

$$\widetilde{\theta} = A\cosh\beta\eta + B\sinh\beta\eta + \widetilde{P}, \tag{14}$$

where the function $\widetilde{P}$ is a particular solution of Eq. (10).

When $\widetilde{\theta}(\eta_i)$ and $\widetilde{\theta}(\eta_{i+1})$ are defined, respectively, as

$$\widetilde{\theta}(\eta_i) = \widetilde{\theta}_i \quad \text{and} \quad \widetilde{\theta}(\eta_{i+1}) = \widetilde{\theta}_{i+1}, \tag{15}$$

the approximation function, Eq. (14), in the interval $[\eta_i, \eta_{i+1}]$ can be written as

$$\widetilde{\theta} = \frac{1}{\sinh\beta\ell}\left[\sinh\beta(\eta-\eta_i)(\widetilde{\theta}-\widetilde{P})_{i+1} + \sinh\beta(\eta_{i+1}-\eta)(\widetilde{\theta}-\widetilde{P})_i\right] + \widetilde{P}. \tag{16}$$

Similarly, the approximation function in the interval $[\eta_{i-1}, \eta_i]$ can be written as

$$\widetilde{\theta} = \frac{1}{\sinh\beta\ell}\left[\sinh\beta(\eta-\eta_{i-1})(\widetilde{\theta}-\widetilde{P})_i + \sinh\beta(\eta_i-\eta)(\widetilde{\theta}-\widetilde{P})_{i-1}\right] + \widetilde{P} \tag{17}$$

Substituting Eqs. (16) and (17) into Eq. (12) and then evaluating the resulting integral can produce the following discretized form for the interior nodes as

$$C_{i-1}\widetilde{\theta}_{i-1} + C_i\widetilde{\theta}_i + C_{i+1}\widetilde{\theta}_{i+1} = F_i \qquad i = 2, 3, \ldots, m-1, \tag{18}$$

where the coefficients C_{i-1}, C_i, and C_{i+1} are given as

$$C_{i-1} = 1, \tag{19a}$$

$$C_i = -2\cosh(\beta\ell), \tag{19b}$$

$$C_{i+1} = 1, \tag{19c}$$

and the forcing term is given as

$$F_i = \widetilde{P}_{i-1} - 2\cosh\beta\ell\ \widetilde{P}_i + \widetilde{P}_{i+1} + \frac{\sinh\beta\ell}{\beta}\left[\int_{\eta_i-\ell/2}^{\eta_i+\ell/2}\left[\beta^2\widetilde{P} - \widetilde{H}\right]d\eta - \frac{d\widetilde{P}}{d\eta}\bigg|_{\eta_i-\ell/2}^{\eta_i+\ell/2}\right]. \tag{20}$$

The resulting integral value of the fourth term in the right side of Eq. (20) would be zero as the function $\widetilde{P}$ is determined to be the particular solution of Eq. (10), and the structure of the governing algebraic equations is simplified.

Rearrangement of Eq. (18) with the appropriate boundary conditions yields the following matrix equation as

$$[C]\left\{\widetilde{\theta}\right\} = \{F\}, \tag{21}$$

where $[C]$ is a matrix with the complex number s, $\left\{\widetilde{\theta}\right\}$ is a matrix representing the unknown dimensionless nodal temperatures in the Laplace transform domain, and $\{F\}$ is a vector representing the forcing term. Thereafter, application of the Gaussian elimination algorithm and the numerical inversion of the Laplace transform [25] to Eq. (21) can yield the nodal temperatures in the physical domain.

4. RESULTS AND DISCUSSION

Numerical results for the hyperbolic two-step heat conduction problems with the insulated boundary condition are developed. The thermal properties for metals at room temperature are shown in Table I. To investigate the effect of the thermal properties on the microscopic thermal behavior in thin metal films, the present results are computed with various values of R_C and N.

Table I. Thermal Properties for Metals at Room Temperature [26]

	Au	Ag	Cu	Cr	W	Pb
$G(TW \cdot m^{-3} \cdot K^{-1})$	28000	28000	48000	420000	260000	120000
$C_e(MJ \cdot m^{-3} \cdot K^{-1})$	0.021	0.019	0.029	0.058	0.041	0.049
$C_l(MJ \cdot m^{-3} \cdot K^{-1})$	2.5	2.5	3.4	3.2	2.5	1.5
$k(W \cdot m^{-1} \cdot K^{-1})$	317	429	401	93.7	174	35.3
τ(ps)	0.04	0.04	0.03	0.003	0.01	0.005

4.1. One End at Constant Temperature and the Other Insulated

It is assumed that the temperature distribution in the sample film is induced with the constant boundary temperature and E is regarded as zero. The boundary conditions are considered as

$$\theta_e(0, \xi) = 1 \quad \text{and} \quad \frac{\partial \theta_e(1, \xi)}{\partial \eta} = 0. \tag{22}$$

As $E = 0$ (i.e., $\widetilde{E} = 0$), Eq. (8a) is a homogeneous differential equation. Applying the Laplace transform to Eq. (22) and using Eq. (8a), the analytical solution of $\widetilde{\theta}_e$ for this case is obtained;

$$\widetilde{\theta}_e = \frac{1}{s}(\cosh \beta\eta - \tanh \beta \sinh \beta\eta), \tag{23}$$

and then the analytical solution of $\widetilde{\theta}_l$ can be obtained from Eqs. (7b) and (23). Numerical inversion of the Laplace transform [25] can be applied to perform the inverse transform of $\widetilde{\theta}_e$ and $\widetilde{\theta}_l$ for θ_e and θ_l.

Table II shows the numerical results of θ_e for $\xi = 0.5$, $R_C = 100$, and $N = 60$, computed with different ℓ values from 0.005 to 0.04. The present results are in good agreement for various ℓ values, that is, the present numerical scheme is not sensitive to the value of ℓ for such a problem. The magnitude of θ_e $(\eta, 0.5)$ drops from the order of 10^{-6} to the order of 10^{-14} in the domain $0.5 \leqslant \eta \leqslant 0.51$. These phenomena imply that the present numerical results are convergent, and the velocity of heat propagation in the hyperbolic two-step model is finite.

Table II. Numerical Values of $\theta_e(\eta, 0.5)$ Computed at Different ℓ Values for the Case of Constant Boundary Temperature

η	0.1	0.2	0.3	0.4	0.5	0.51
θ_e	0.40494	0.10180	0.01285	0.00050	1×10^{-6}	-1×10^{-14}

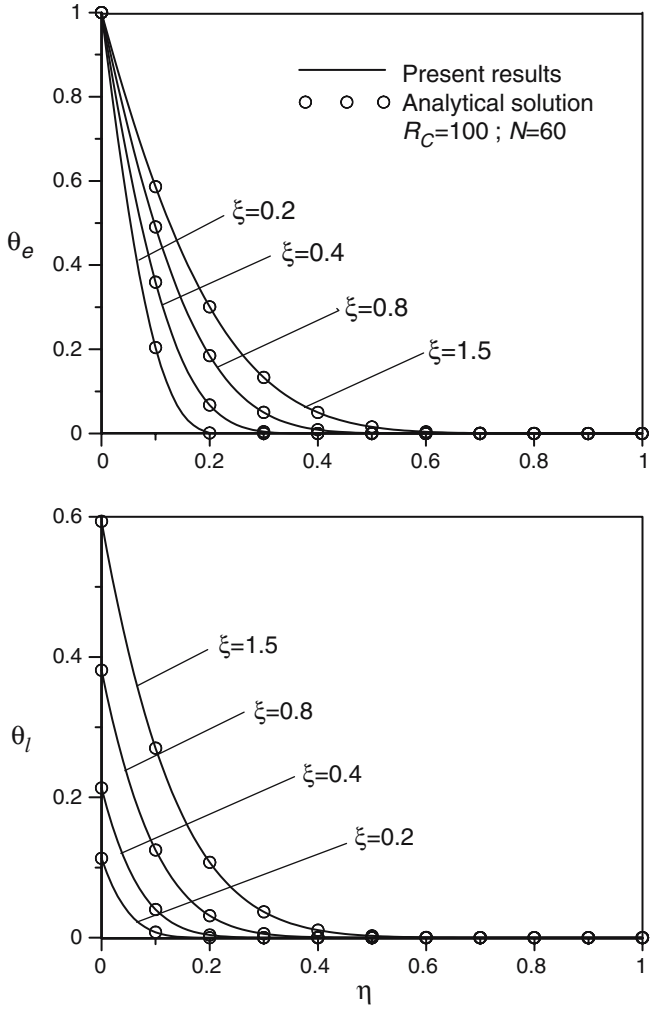

Fig. 1. Distributions of electron and lattice temperatures at different times with $R_C = 100$ and $N = 60$ for the case of constant boundary temperature.

Figure 1 presents the distributions of electron and lattice temperatures for various ξ values with $R_C = 100$ and $N = 60$. To demonstrate the accuracy and consistency of the present numerical method, a comparison of the dimensionless temperature distribution between the present numerical results and the analytical solution is also shown. The present numerical results agree well with the analytical solution. It is found that the

magnitude of the dimensionless temperature distribution increases as the value of ξ increases. This is because the heat flux from the end at $\eta = 0$ continually enters into the sample film since $\xi > 0$. However, due to the diffusion and coupling effects, the increasing rate in the magnitude of the electron and lattice temperatures gradually decreases with an increase in the value of ξ.

In order to know the effect of the coupling factor on the hyperbolic two-step heat conduction, Fig. 2 displays the distributions of θ_e for various N values at $R_C = 100$ and $\xi = 0.5$. It is explained from the definition of N that the value of N is proportional to the coupling factor. In other words, the amount of energy exchange between electrons and phonons would be proportional to the value of N. The rate of energy exchange decreases with a decrease in the value of N. The magnitude of the electron temperature distribution is higher for a smaller value of N, as shown in Fig. 2. It also can be found from the results in Fig. 2 that the effect of the coupling factor on the dimensionless electron temperature distribution for $R_C = 100$ and $\xi = 0.5$ is reduced with an increase in the value of N.

Figure 3 shows the dimensionless electron temperature distribution for various R_C values at $N = 60$ and $\xi = 0.5$. R_C is the volumetric heat capacity ratio and is defined as $R_C = C_l / C_e$. As the value of R_C increases, the value of C_l increases and the lattice can accumulate more energy.

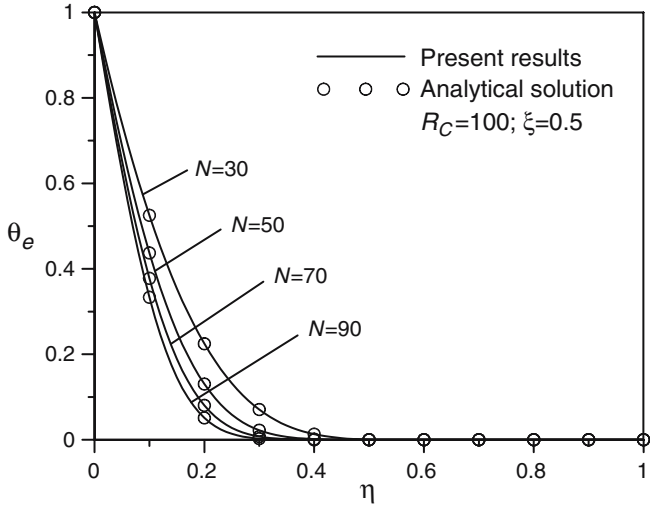

Fig. 2. Comparison between the present numerical results and the analytical solution at different N values for the case of constant boundary temperature.

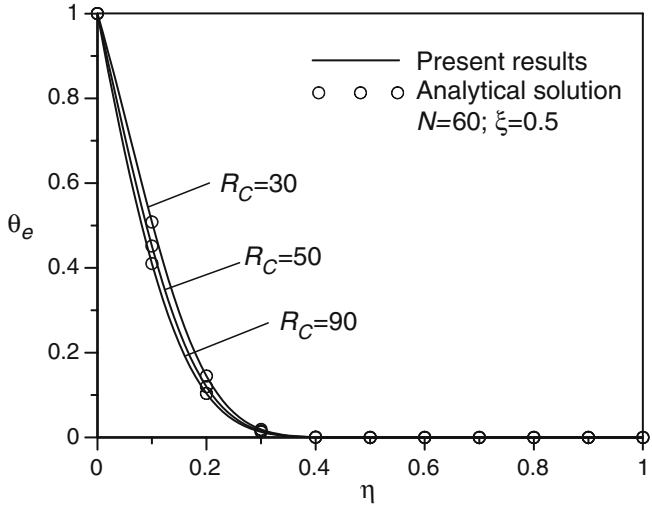

Fig. 3. Comparison between the present numerical results and the analytical solution at different R_C values for the case of constant boundary temperature.

Thus, the lattice temperature has a relatively low value for the larger value of R_C. Energy exchange between electrons and phonons is easier, and there is a lower electron temperature as shown in Fig. 3. Figures 2 and 3 also show the comparison of the dimensionless temperature distribution between the present numerical results and the analytical solution. The result further demonstrates the accuracy of the present results.

4.2. Application of Strong Energy Pulse at the End

Assume an impulse energy source that is totally absorbed by the electron gas is released at $\xi = 0$ and at the end $\eta = 0$. The other end, $\eta = 1$, is insulated. The boundary conditions, thus, are described as

$$Q(0, \xi) = \delta(\xi) \quad \text{and} \quad \frac{\partial \theta_e(1, \xi)}{\partial \eta} = 0, \tag{24}$$

where δ is the Dirac function.

Applying the Laplace transform to Eq. (24) can result in the transformed boundary conditions as

$$\frac{d\widetilde{\theta}_e(0)}{d\eta} = -(s+1) \quad \text{and} \quad \frac{d\widetilde{\theta}_e(1)}{d\eta} = 0. \tag{25}$$

Therefore, by using Eq. (8a) with $\widetilde{E}=0$, an analytical solution of $\widetilde{\theta}_e$ can be obtained;

$$\widetilde{\theta}_e = \frac{(s+1)\cosh\beta\cosh\beta\eta}{\beta\sinh\beta} - \frac{(s+1)\sinh\beta\eta}{\beta}. \tag{26}$$

Similarly, an analytical solution of $\widetilde{\theta}_l$ can be obtained from Eqs. (7b) and (26), and performing the inverse transform of $\widetilde{\theta}_e$ and $\widetilde{\theta}_l$ leads to the values of θ_e and θ_l.

Figure 4 shows the spatial variation of both electron and lattice temperatures induced with the application of a strong energy pulse at different ξ values for $R_C=100$ and $N=60$. It is found from Fig. 4 that the energy pulse gradually decays with an increase in the value of ξ due to the electron–phonon interaction and the diffusion in the electron gas. In addition, it is observed from the electron temperature distribution that the locations of the energy pulse are at $\eta=0.2$ and 0.4 for $\xi=0.2$ and 0.4, respectively. This phenomenon implies that heat transfers at a finite velocity based on the hyperbolic two-step model. At the same time, the location of the energy pulse is the depth of the thermal signal penetrating into the film and is equal to tV. Thus, in accordance with the definition of η and ξ, the velocity of heat transfer can be converted to $V=\sqrt{k/(C_e\tau)}$, similar to that for the hyperbolic one-step model. Due to the Dirac's functional form of the heating source, the energy pulses at $\eta=0.2$ and 0.4 for $\xi=0.2$ and 0.4, respectively, are sharp. The primary difficulty in dealing with this case is the suppression of numerical oscillations in the vicinity of the sharp discontinuity. The results show that the present numerical results agree well with the analytical solution and do not exhibit numerical oscillations in the vicinity of the jump discontinuity. Al-Nimr et al. [15] solved a similar case with a perturbation technique under the assumption that the difference between the temperatures of electrons and the lattice is sufficiently small. Their results show that the perturbation technique fails near $\eta=0$ and $\xi=0$. However, the present results satisfy the boundary conditions and agree well with the analytical solution. Obviously, the present numerical scheme is stable and accurate for such problems.

In order to explore further the effect of the coupling factor on the solution of the hyperbolic two-step heat conduction equations, Fig. 5 shows the distributions of the dimensionless electron temperature at $\xi=0.5$ for various N values and $R_C=100$. The value of N is proportional to the coupling factor. Thus, the energy pulse has been weak at $N=50$ and 90 for the electron–phonon interaction. In addition, the location of the energy pulse at a specific dimensionless time is the same for various N values. This phenomenon further implies that the propagation velocity of

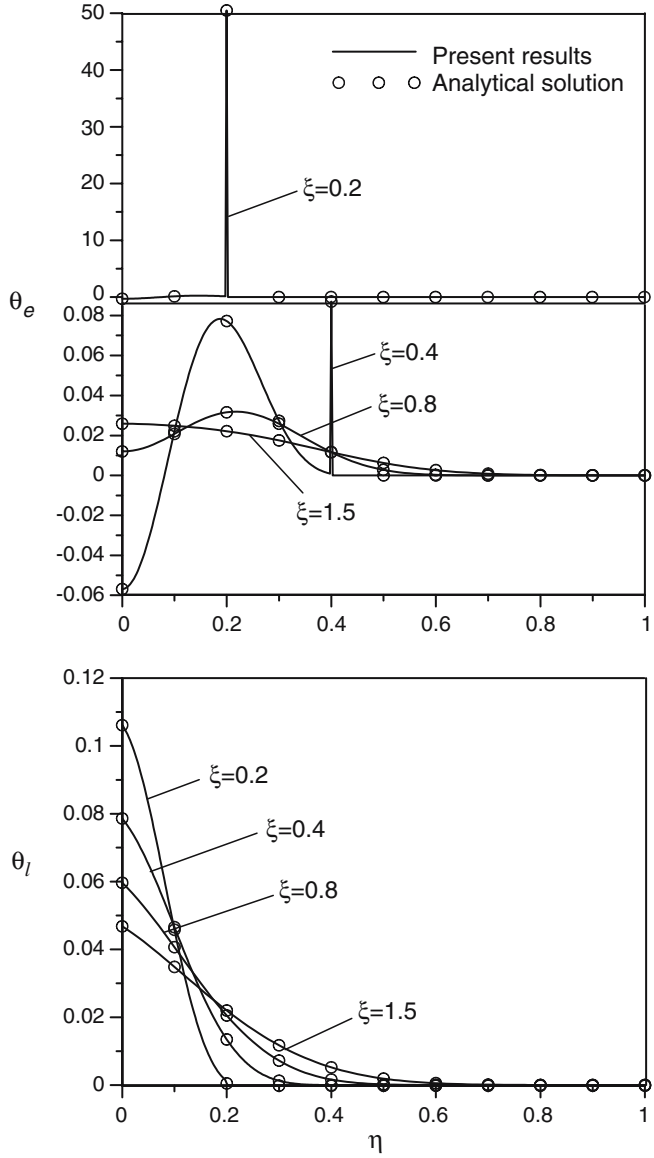

Fig. 4. Distributions of electron and lattice temperatures at different times with $R_C = 100$ and $N = 60$ for the case of application of strong energy pulse.

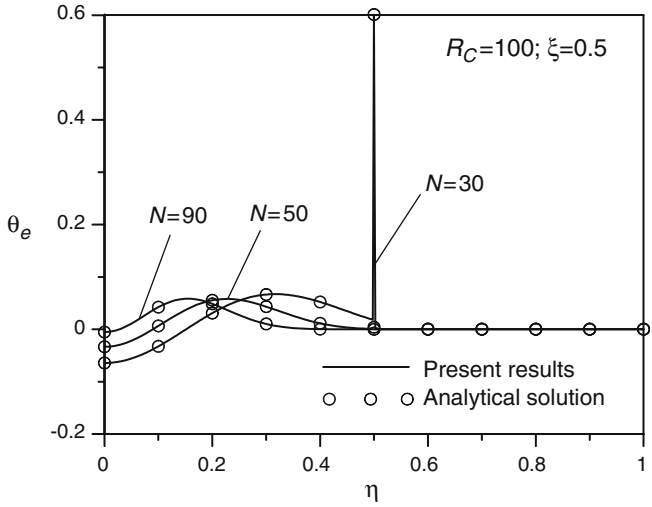

Fig. 5. Comparison between the present numerical results and the analytical solution at different N values for the case of application of strong energy pulse.

the thermal signal based on the hyperbolic two-step model can be defined as $V = \sqrt{k/(C_e \tau)}$ and is independent of the value of N.

Figure 6 shows the dimensionless electron temperature distributions for the situations described in Fig. 3. It is obvious that the strength of the energy pulse shown in Fig. 6 is very weak. However, it can be clearly observed that the location of the energy pulse at a specific dimensionless time is also the same for various R_C values. This result demonstrates that the propagation velocity of the thermal signal is also independent of the R_C value. The results illustrated in Figs. 5 and 6 imply that the propagation velocity of the thermal signal depends only on the thermal diffusivity, k/C_e, and the relaxation time τ. Furthermore, the electron temperature is at a relatively low value for the larger value of R_C. It is the same as that shown in Fig. 3.

4.3. Exponentially Decaying Heat Source

In this section, the thermal behavior induced by an exponentially decaying internal source is analyzed. The internal source is considered as an exponential function of η and ξ such that $E(\eta, \xi)$ is given by

$$E(\eta, \xi) = e^{-\eta - \xi}, \tag{27}$$

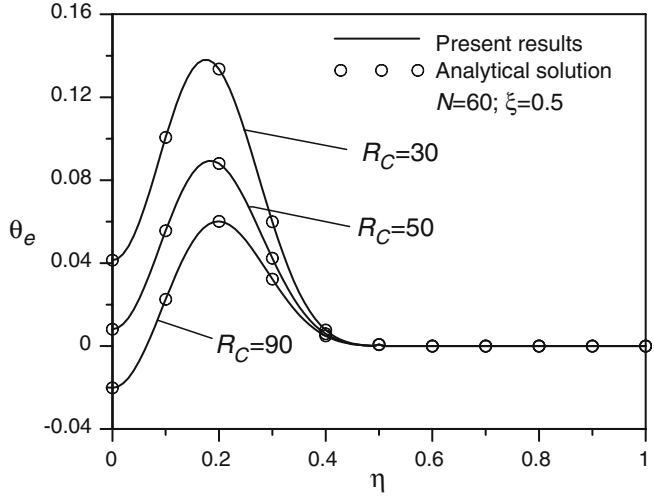

Fig. 6. Comparison between the present numerical results and the analytical solution at different R_C values for the case of application of strong energy pulse.

and then

$$\widetilde{E} = \frac{1}{s+1} \mathrm{e}^{-\eta}. \tag{28}$$

Therefore, the force term in Eq. (8a) cannot be neglected in this case. For obtaining accurate numerical results, the function $\widetilde{P}$ is considered as

$$\widetilde{P} = \frac{1}{\beta^2 - 1} \mathrm{e}^{-\eta}. \tag{29}$$

As the sample film is subjected to the boundary conditions,

$$\frac{\partial \theta_{\mathrm{e}}(0, \xi)}{\partial \eta} = 0 \quad \text{and} \quad \frac{\partial \theta_{\mathrm{e}}(1, \xi)}{\partial \eta} = 0, \tag{30}$$

the analytical solution of $\widetilde{\theta}_{\mathrm{e}}$ can be written as

$$\widetilde{\theta}_{\mathrm{e}} = \frac{1}{\beta(\beta^2 - 1)} \sinh \beta\eta + \frac{e^{-1} - \cosh \beta}{\beta(\beta^2 - 1) \sinh \beta} \cosh \beta\eta + \frac{1}{\beta^2 - 1} \mathrm{e}^{-\eta}. \tag{31}$$

The analytical solution of $\widetilde{\theta}_{\mathrm{l}}$ is also obtained from Eqs. (7b) and (31), and the values of θ_{e} and θ_{l} are computed through the Laplace transform.

A comparison between the present numerical results and the analytical solution is presented in Fig. 7. The present numerical results also agree well with the analytical solution and satisfy the boundary conditions. This result demonstrates further the efficiency and accuracy of the present numerical scheme for solving the coupled equations of the hyperbolic two-step model. It is observed from Fig. 7 that the electron gas has a higher

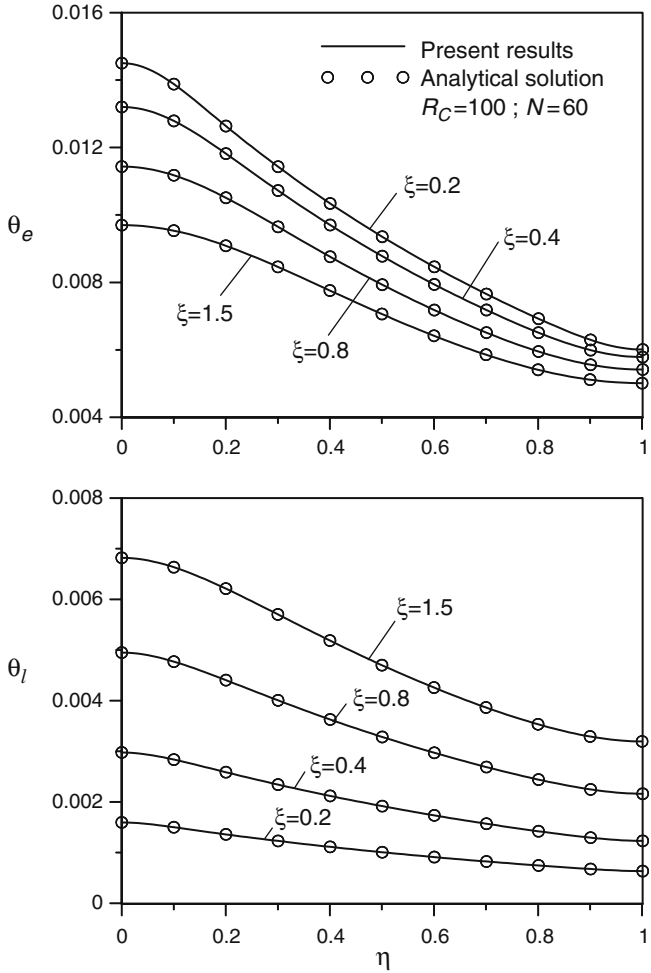

Fig. 7. Distributions of electron and lattice temperatures at different times with $R_C = 100$ and $N = 60$ for the case of exponentially decaying heat source.

temperature for $\xi \leqslant 1.5$ due to the fact that the electron gas absorbs the energy first. But, both electron and lattice temperatures approach a state of equilibrium with the value of ξ increasing for the coupling effect.

5. CONCLUSIONS

This work analyzes various microscopic heat transfer problems in a sample film with an insulated boundary surface using the hyperbolic two-step model. The present numerical results show no remarkable difference with the analytical solution. It demonstrates the accuracy of the present numerical scheme for such problems. Results further imply that the propagation velocity of the thermal signal, based on the hyperbolic two-step model, is also finite and is independent of the values of N and R_C. However, there is no obvious thermal wave front depicted in the hyperbolic one-step heat conduction, even when the heat source is described with Dirac's function, due to the electron–phonon interactions.

NOMENCLATURE

C	volumetric heat capacity
E	dimensionless heating source, defined as $E = \dfrac{S\tau}{C_e T_r}\widetilde{E}$
$\widetilde{E}$	Laplace transform of E
G	coupling factor
k	thermal conductivity
ℓ	distance between neighboring nodes
N	parameter, defined as $N = \dfrac{G\tau}{C_e}$
Q	dimensionless heat flux, defined as $Q = \dfrac{q}{T_r\sqrt{kC_e/\tau}}$
$\widetilde{Q}$	Laplace transform of Q
q	heat flux
R_C	parameter, defined as $R_C = \frac{C_l}{C_e}$
S	heating source
s	Laplace transform parameter
T	temperature
T_0	initial temperature
T_r	reference temperature
t	time
V	propagation speed of thermal signal, defined as $V = \sqrt{k/C_e\tau}$
x	space coordinate

Greek Symbols

β parameter, defined in Eq. (9)

η dimensionless space coordinate, defined as $\eta = \dfrac{x}{\sqrt{k\tau/C_e}}$

θ dimensionless temperature, defined as $\theta = \dfrac{T - T_0}{T_r}$

$\widetilde{\theta}$ Laplace transform of θ

ξ dimensionless time, defined as $\xi = \dfrac{t}{\tau}$

τ relaxation time

Subscripts

e electron

i node number

l lattice

REFERENCES

1. J. G. Fujimoto, J. M. Liu, and E. P. Ippen, *Phys. Rev.* **53**:416 (1984).
2. S. D. Brorson, J. G. Fujimoto, and E. P. Ippen, *Phys. Rev. Lett.* **59**:1962 (1987).
3. H. E. Elsayed-Ali, *Phys. Rev.* **B43**:4488 (1991).
4. M. I. Kaganov, I. M. Lifshitz, and L. V. Tanatarov, *Sov. Phys. JETP* **4**:173 (1957).
5. S. I. Anisimov, B. L. Kapeliovich, and T. L. Perel'man, *Sov. Phys. JETP* **39**:375 (1974).
6. H. E. Elsayed-Ali, T. B. Norris, M. A. Pessot, and G. A. Mourou, *Phys. Rev. Lett.* **58**:1212 (1987).
7. P. B. Corkum, F. Brunel, and N. K. Sherman, *Phys. Rev. Lett.* **61**:2886 (1987).
8. T. Q. Qiu and C. L. Tien, *Int. J. Heat Mass Transfer* **35**:719 (1992).
9. T. Q. Qiu and C. L. Tien, *Int. J. Heat Mass Transfer* **37**:2789 (1994).
10. S. Kiwan and M. A. Al-Nimr, *Jpn. J. Appl. Phys.* **39**:4245 (2000).
11. M. A. Al-Nimr, M. Hader, and M. Naji, *Int. J. Heat Mass Transfer* **46**:333 (2003).
12. T. Q. Qiu and C. L. Tien, *J. Heat Transfer* **115**:835 (1993).
13. D. Y. Tzou, *Int. J. Heat Mass Transfer* **38**:3231 (1995).
14. M. A. Al-Nimr and V. S. Arpaci, *Int. J. Heat Mass Transfer* **43**:2021 (2000).
15. M. A. Al-Nimr, O. M. Haddad, and V. S. Arpaci, *Heat Mass Transfer* **35**:459 (1999).
16. M. Naji, M. A. Al-Nimr, and M. Hader, *Int. J. Thermophys.* **24**:545 (2003).
17. M. A. Al-Nimr and M. K. Alkam, *Int. J. Thermophys.* **24**:577 (2003).
18. D. Y. Tzou, *ASME J. Heat Transfer* **117**:8 (1995).
19. D. Y. Tzou, *Macro- to Microscale Heat Transfer: The Lagging Behavior*, (Taylor & Francis, Washington, DC, 1997). Chap. 10.
20. D. Y. Tzou, *ASME J. Dynamic Systems, Measurement, and Control* **125**:563 (2003).
21. T. M. Shih, *Numerical Heat Transfer* (Hemisphere, New York, 1984), p. 55.
22. H. T. Chen and K. C. Liu, *Int. J. Heat Mass Transfer* **46**:2809 (2003).
23. H. T. Chen and K. C. Liu, *Comput. Phys. Commun.* **150**:31 (2003).
24. H. T. Chen and K. C. Liu, *Int. J. Numer. Methods Eng.* **57**:637 (2003).
25. G. Honig and U. Hirdes, *J. Comput. Appl. Math.* **10**:113 (1984).
26. K. J. Hays-Stang and A. Haji-Sheikh, *Int. J. Heat Mass Transfer* **42**:455 (1999).